AMERICAN SOCIETY FOR MICROBIOLOGY | mBio®

RESEARCH ARTICLE

A Cysteine Pair Controls Flavin Reduction by Extracellular Cytochromes during Anoxic/Oxic Environmental Transitions

Michael P. Norman,[a] Marcus J. Edwards,[b] Gaye F. White,[c] Joshua A. J. Burton,[c] Julea N. Butt,[c] David J. Richardson,[c] Ricardo O. Louro,[d] Catarina M. Paquete,[d] Thomas A. Clarke[c]

[a]Babraham Institute, Babraham Research Campus, Babraham, Cambridge, United Kingdom
[b]School of Life Sciences, University of Essex, Colchester, United Kingdom
[c]School of Biological Sciences and School of Chemistry, University of East Anglia, Norwich, United Kingdom
[d]Instituto de Tecnologia Química e Biológica António Xavier, Universidade NOVA de Lisboa, Oeiras, Portugal

ABSTRACT Many bacteria of the genus *Shewanella* are facultative anaerobes able to reduce a broad range of soluble and insoluble substrates, including Fe(III) mineral oxides. Under anoxic conditions, the bacterium *Shewanella oneidensis* MR-1 uses a porin-cytochrome complex (Mtr) to mediate extracellular electron transfer (EET) across the outer membrane to extracellular substrates. However, it is unclear how EET prevents generating harmful reactive oxygen species (ROS) when exposed to oxic environments. The Mtr complex is expressed under anoxic and oxygen-limited conditions and contains an extracellular MtrC subunit. This has a conserved CX_8C motif that inhibits aerobic growth when removed. This inhibition is caused by an increase in ROS that kills the majority of *S. oneidensis* cells in culture. To better understand this effect, soluble MtrC isoforms with modified CX_8C were isolated. These isoforms produced increased concentrations of H_2O_2 in the presence of flavin mononucleotide (FMN) and greatly increased the affinity between MtrC and FMN. X-ray crystallography revealed that the molecular structure of MtrC isoforms was largely unchanged, while small-angle X-ray scattering suggested that a change in flexibility was responsible for controlling FMN binding. Together, these results reveal that FMN reduction in *S. oneidensis* MR-1 is controlled by the redox-active disulfide on the cytochrome surface. In the presence of oxygen, the disulfide forms, lowering the affinity for FMN and decreasing the rate of peroxide formation. This cysteine pair consequently allows the cell to respond to changes in oxygen level and survive in a rapidly transitioning environment.

IMPORTANCE Bacteria that live at the oxic/anoxic interface have to rapidly adapt to changes in oxygen levels within their environment. The facultative anaerobe *Shewanella oneidensis* MR-1 can use EET to respire in the absence of oxygen, but on exposure to oxygen, EET could directly reduce extracellular oxygen and generate harmful reactive oxygen species that damage the bacterium. By modifying an extracellular cytochrome called MtrC, we show how preventing a redox-active disulfide from forming causes the production of cytotoxic concentrations of peroxide. The disulfide affects the affinity of MtrC for the redox-active flavin mononucleotide, which is part of the EET pathway. Our results demonstrate how a cysteine pair exposed on the surface controls the path of electron transfer, allowing facultative anaerobic bacteria to rapidly adapt to changes in oxygen concentration at the oxic/anoxic interface.

KEYWORDS peroxide, flavoprotein, flavin, *Shewanella oneidensis*, cytochrome, cysteine

The facultative anaerobe *Shewanella oneidensis* MR-1 expresses a broad range of multiheme cytochromes that allow it to utilize a diverse range of substrates as terminal electron acceptors (1). These acceptors include soluble molecules such as dimethyl sulfoxide and nitrate and insoluble substrates such as Fe(III) and Mn(IV) oxides (2–4).

Editor Richard Gerald Brennan, Duke University School of Medicine

Address correspondence to Thomas A. Clarke, tom.clarke@uea.ac.uk.

The authors declare no conflict of interest.

Received 30 September 2022
Accepted 19 December 2022

The central mechanism for electron transfer across the membrane involves the Mtr complex, a porin-cytochrome complex that consists of periplasmic decaheme MtrA, a large transmembrane pore MtrB, and the decaheme cytochrome MtrC on the surface of the cell (5). This Mtr complex forms an electron conduit through the outer membrane of *Shewanella* where MtrA directly exchanges electrons with the associated MtrC (6, 7). MtrC is extended approximately 80 Å above the lipid bilayer of the cell membrane, providing a surface for extracellular electron transfer to environmental substrates (7, 8).

While deletion of both MtrC and the analogous OmcA prevents the reduction of extracellular iron oxides, iron reduction by *S. oneidensis* is also dependent on the secretion of nanomolar concentrations of flavins (9, 10). These flavins can function as soluble shuttles, transporting electrons between extracellular cytochromes and the mineral surface. Reduction of certain iron oxides, such as ferrihydrite and lepidocrocite, by reduced flavin has been shown to occur at favorable rates (11). However, soluble reduced flavin mononucleotide (FMN) is a poor chemical reductant of mineral species such as hematite and goethite, and these minerals might be directly reduced by the extracellular cytochromes (12).

In addition to functioning as a soluble mediator, FMN has been shown to associate with MtrC and OmcA. *In vitro* studies of both oxidized MtrC and OmcA showed that these cytochromes were capable of interacting with FMN or riboflavin, although the dissociation constants obtained suggested that the interaction between MtrC and OmcA was likely to be transient, rather than stable (13). Theoretical binding sites have also been proposed on the surface of MtrC that are within electron transfer distance of adjacent heme groups (14–16).

MtrC is composed of four domains: an N-terminal β-barrel domain (domain I) is followed by a pentaheme domain (domain II), a second β-barrel domain (domain III), and a C-terminal pentaheme domain (domain IV). Domain III contains a conserved CX_8C motif, which forms a disulfide bond between the two cysteines (17). Reduction of MtrC with glutathione caused a change in affinity for FMN, and cells expressing a plasmid-based *mtrC* with codons substituted to change the CX_8C motif to AX_8A were unable to grow aerobically. Disulfide bonds are often used as redox switches to regulate protein activity in different oxidative environments (18, 19), but it is unclear how the MtrC disulfide could be linked to both FMN association and the ability of *S. oneidensis* to respond to the presence of oxygen.

To investigate this, we analyzed the effects of site-directed mutagenesis on MtrC and show that removal of the disulfide causes global changes in the domain structure of MtrC that alter the affinity of MtrC for FMN. This modification produces cytotoxic levels of hydrogen peroxide under aerobic conditions while allowing mineral reduction under anoxic conditions. These results indicate that the MtrC disulfide acts as an oxygen sensor by disconnecting the EET chain to flavin in the presence of oxygen, thereby limiting formation of reactive oxygen that could otherwise damage the cell.

RESULTS

Synthesis of *MtrC* containing a modified CX_8C motif restricts growth under aerobic conditions. *S. oneidensis* Δ*mtrC* was transformed with the plasmid vectors shown in Table S1 in the supplemental material to make mutant *S. oneidensis* strains that would produce MtrC with modified CX_8C motifs (Table 1). These strains were *S. oneidensis* pMtrC (CX_8C), *S. oneidensis* pC444A (AX_8C), *S. oneidensis* pC453A (CX_8A), and *S. oneidensis* pC444A, C453A (AX_8A). In the absence of the inducing agent, arabinose, all four strains showed similar growth under aerobic conditions (Fig. 1A). However, addition of 5 mM or 10 mM arabinose caused the *S. oneidensis* strains containing genes with a modified CX_8C motif to exhibit biphasic growth (Fig. 1B and C). Initially, all strains enter a similar exponential phase for approximately 2 h, but then, growth of strains with a modified CX_8C motif becomes arrested, with *S. oneidensis* pC453A being the most significantly affected. This continues for approximately 10 h before growth resumes and all strains reach the same final optical density (OD) after 24 h. Addition of arabinose to the same *S. oneidensis* strains did not affect the ability to grow under

TABLE 1 *S. oneidensis* strains used in this study

Name	Host strain	Plasmid	Note(s)
S. oneidensis MR-1	*S. oneidensis* MR-1		
S. oneidensis ΔmtrC	*S. oneidensis* ΔmtrC		
S. oneidensis pMtrC	*S. oneidensis* ΔmtrC	pMtrC	CX_8C motif
S. oneidensis pC453A	*S. oneidensis* ΔmtrC	pC453A	CX_8A motif
S. oneidensis pC444A	*S. oneidensis* ΔmtrC	pC444A	AX_8C motif
S. oneidensis pC444A, C453A	*S. oneidensis* ΔmtrC	pC444A, C453A	AX_8A motif
S. oneidensis pMtrCsol	*S. oneidensis* ΔmtrC	pMtrCsol	Soluble form, CX_8C motif
S. oneidensis pC453Asol	*S. oneidensis* ΔmtrC	pC453Asol	Soluble form, CX_8A motif
S. oneidensis pC453Ssol	*S. oneidensis* ΔmtrC	pC453Ssol	Soluble form, CX_8S motif

anaerobic conditions (Fig. S1), indicating that exposure to oxygen was responsible for the arrest in growth.

The relative levels of synthesis of each modified MtrC were measured. SDS-PAGE revealed that the presence of $MtrC_{C453A}$ was significantly higher than either $MtrC_{C444A}$ or $MtrC_{C444A,C453A}$ (Fig. S2A) and was consistent with the more severe phenotype observed for *S. oneidensis* pC453A. Together, these data show that synthesis of MtrC with a modified CX_8C motif limits cell growth under aerobic conditions. After 24 h of growth, the number of all MtrC isoforms in the membrane fractions was significantly less (Fig. S2B), indicating that expression of plasmid-based *mtrC* mutants had ceased.

$MtrC_{C453A}$ was isolated using affinity chromatography as part of a stable Mtr complex, indicating that it could function as an electron acceptor for periplasmic MtrA and play a role in EET (Fig. S3A). To confirm that the $MtrC_{C453A}$ was functional as an electron transport protein, the reduction rate of the Fe(III) mineral goethite was measured (Fig. S3B). The *S. oneidensis* Δ*mtrC* strain was unable to release Fe(II) from goethite, while the Fe(II) formation for both *S. oneidensis* pC453A and *S. oneidensis* pMtrC was the same, indicating that in these experiments, the role of MtrC in mineral reduction was not affected by substitution of Cys_{453}.

The formation of cytotoxic hydrogen peroxide is responsible for limiting *S. oneidensis* growth. Cytotoxic effects of oxygen are typically linked to the reduction of oxygen to the reactive oxygen species (ROS), superoxide ($O_2^{\bullet -}$), peroxide (O_2^{2-}), and hydroxyl radical (HO•). Peroxide is the most stable of these species and forms hydrogen peroxide (H_2O_2) under aqueous conditions at neutral pH. The formation of peroxide or superoxide by *S. oneidensis* pC453A was measured by adding the enzymes catalase or superoxide dismutase to aerobically growing cells (Fig. 2A and B). The addition of catalase allowed aerobic growth at a similar rate to *S. oneidensis* pMtrC, while the addition of superoxide dismutase had no effect on the aerobic growth profile. These results suggest that direct $2e^-$ reduction of oxygen to hydrogen peroxide, rather than superoxide, is responsible for the growth phenotype of the *S. oneidensis* pC453A mutant.

The concentration of hydrogen peroxide formed was measured by growing *S. oneidensis* strains overnight under anaerobic conditions using fumarate as an electron acceptor. The cultures were then exposed to air for 3 h, and the hydrogen peroxide concentration in the media was measured. The concentrations of hydrogen peroxide in air-exposed *S. oneidensis* pMtrC and *S. oneidensis* pC453A were 61 $\pm$ 36 μM and 257 $\pm$ 71 μM, respectively, revealing a 4-fold-higher concentration of hydrogen peroxide in the culture containing cells expressing $MtrC_{C453A}$. *S. oneidensis* pMtrC and *S. oneidensis* pC453A grown aerobically for 24 h contained 39 $\pm$ 9 μM and 19 $\pm$ 3 μM hydrogen peroxide, respectively, indicating that hydrogen peroxide levels had become low enough to allow growth again, consistent with growth of *S. oneidensis* pC453A after the arrested growth phase.

The observed lag phase of cell cultures of *S. oneidensis* synthesizing $MtrC_{C453A}$ (Fig. 2A and B) could be due to either the cells being alive but failing to divide or the cells actively dying in the presence of peroxide. To determine the number of viable cells, aerobic cultures of *S. oneidensis* pMtrC and *S. oneidensis* pC453A were sampled before and after induction with 5 mM arabinose (Fig. 2C). The number of cells in both cultures was approximately equal before induction; however, after 3 h, the number of

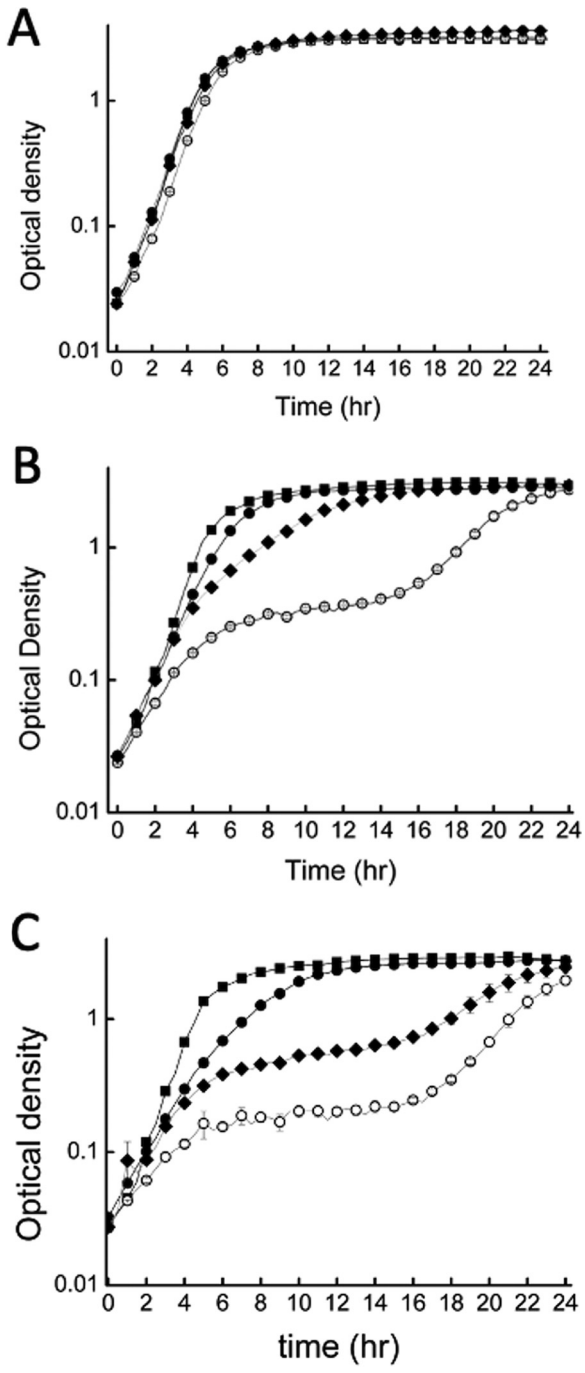

FIG 1 Semilog aerobic growth profiles of *S. oneidensis* pMtrC (squares), *S. oneidensis* pC444A (closed circles), *S. oneidensis* pC453A (open circles), and *S. oneidensis* pC444A, C453A (diamonds) induced with 0 mM arabinose (A), 5 mM arabinose (B), and 10 mM arabinose (C). All strains were grown aerobically in LB supplemented with 50 μg/mL of kanamycin at 30°C.

viable *S. oneidensis* pC453A cells was 30 times lower than the starting number and over 100 times lower than the corresponding *S. oneidensis* pMtrC culture grown for the same length of time. This confirmed that induced synthesis of $MtrC_{C453A}$ caused the death of *S. oneidensis* pC453A in the presence of oxygen, rather than suppression of cell division. Finally, to establish whether 250 μM H_2O_2 was cytocidal, cultures of *S. oneidensis* MR-1 cells were incubated with 100 or 250 μM H_2O_2 and spread onto plates (Fig. 2D). Exposure of *S. oneidensis* MR-1 to 250 μM H_2O_2 for 15 min was sufficient to kill 99% of cells, confirming that the elevated concentrations of H_2O_2 generated during

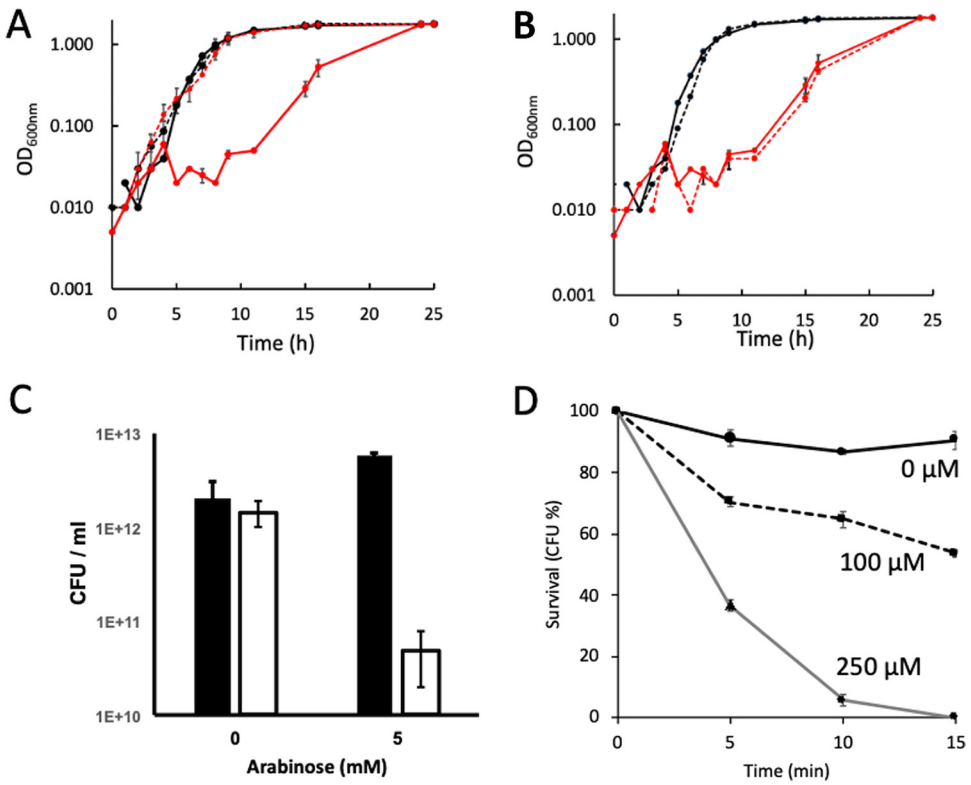

FIG 2 Effect of oxygen species on *S. oneidensis* cells in LB media supplemented with 5 mM arabinose and 50 μg/mL kanamycin. (A) Aerobic growth of *S. oneidensis* pMtrC (black lines) and *S. oneidensis* pC453A (red lines) in the presence (dashed lines) or absence (straight lines) of 0.3 U/mL of catalase. (B) Aerobic growth of *S. oneidensis* pMtrC (black lines) and *S. oneidensis* pC453A (red lines) in the presence (dashed lines) or absence (straight lines) of 0.3 U/mL of superoxide dismutase. (C) Cell viability after 3 h of induction with arabinose. Black bars represent *S. oneidensis* pMtrC; white bars indicate *S. oneidensis* pC453A. (D) Survival of *S. oneidensis* MR-1 in the presence of H_2O_2 as indicated. Error bars represent the standard error of four replicate experiments.

aerobic growth of *S. oneidensis* pC453A were sufficiently high to cause the observed lag phase and subsequent cell death.

Biochemical analysis of isolated MtrC C453A. The *in vivo* data presented in Fig. 1 and 2 revealed that substituting Cys_{453} for alanine resulted in an *S. oneidensis* mutant that generated cytotoxic H_2O_2 under aerobic conditions, effectively turning a facultative anaerobe into a strict anaerobe that recovers by suppressing expression of the plasmid-based *mtrC*. The MtrC crystal structure showed that Cys_{453} forms a disulfide bond with Cys_{444} (17), but it is unclear how preventing the formation of this disulfide bond would increase the catalytic reduction of oxygen to H_2O_2. To resolve this, the soluble forms of both MtrC ($MtrC_{sol}$) and MtrC C453A ($MtrC_{C453Asol}$) were isolated. These constructs lacked the N-terminal LXXC lipid anchor motif and contained a C-terminal StrepTactin tag for ease of purification. The absorbance spectrum of isolated $MtrC_{C453Asol}$ was identical to the absorbance profile of $MtrC_{sol}$, consistent with all hemes having been correctly incorporated and no additional cofactors (Fig. S4A).

To determine whether the reduced form of either $MtrC_{sol}$ or $MtrC_{C453Asol}$ could generate peroxide, 0.5-μM samples of each MtrC variant were reduced by titration with sodium dithionite under anaerobic conditions and then oxidized by exposure to air (Fig. 3A). The amount of hydrogen peroxide generated by both MtrC variants was similar, with a peroxide/electron efficiency of ~0.2%, assuming that 0.5 μM reduced MtrC contained 5 μM reduced hemes. This suggested that direct reduction of O_2 by either MtrC was not the cause of the observed peroxide increase. These experiments were repeated in the presence of 0.1 μM FMN. For $MtrC_{sol}$, the presence of FMN doubled the amount of peroxide formed, while for $MtrC_{C453Asol}$, there was a greater than 5-fold increase in the amount of peroxide formed, with a peroxide/electron efficiency of ~1%. These data reveal that FMN-catalyzed reduction of oxygen is the most likely reason for the observed increase in peroxide formation by cells producing $MtrC_{C453A}$, most

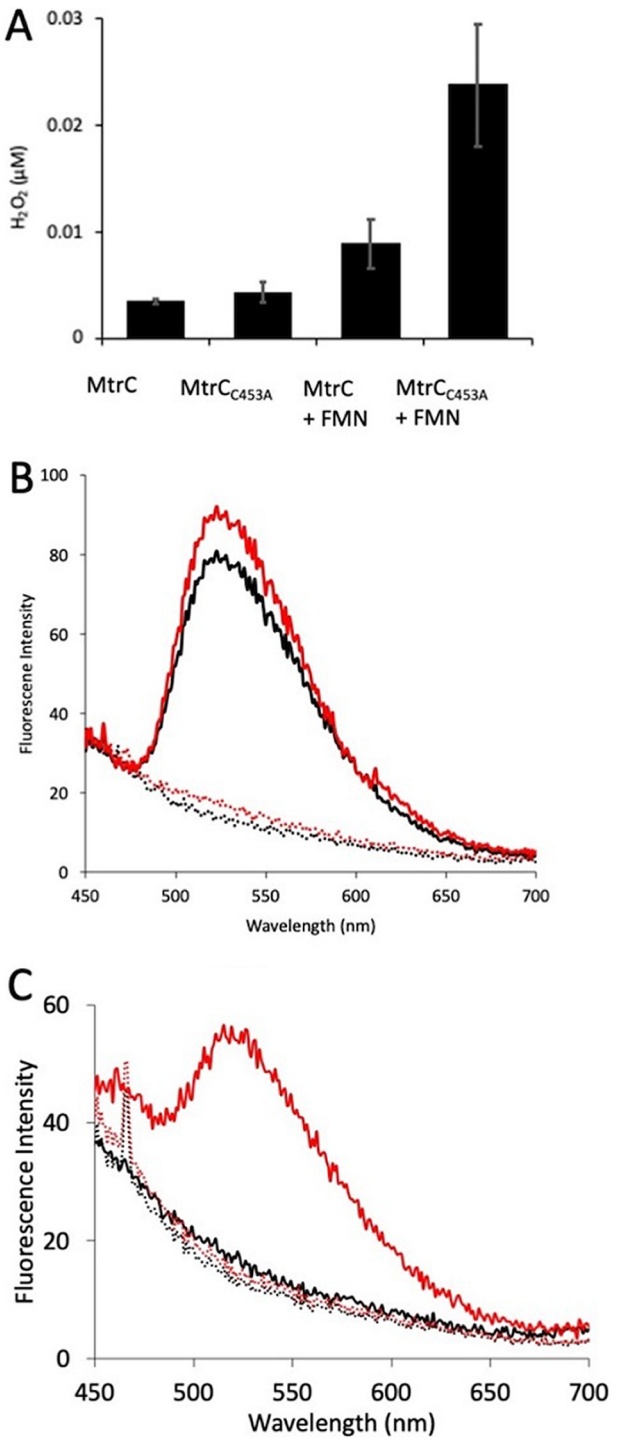

FIG 3 Interactions of FMN with $MtrC_{sol}$ and $MtrC_{C453Asol}$. (A) H_2O_2 generated by 0.5 μM reduced $MtrC_{sol}$ or $MtrC_{C453A\text{-}sol}$ in the presence or absence of 0.1 μM oxidized FMN after exposure to oxygen. (B) Fluorescence spectra of $MtrC_{sol}$ (black) and $MtrC_{C453A\text{-}sol}$ (red) samples incubated with 0 mM (dotted lines) or 1 mM DTT (solid lines) after elution through anaerobic PD10 size exclusion column under anaerobic conditions. Excitation held at 365 nm. (C) Fluorescence spectra of $MtrC_{sol}$ (black) and $MtrC_{C453A\text{-}sol}$ (red) samples incubated with 0 (dotted lines) or 50 μM sodium dithionite (solid lines) after elution through an anaerobic PD10 size exclusion column under anaerobic conditions.

likely due to a change in the interaction between FMN and $MtrC_{C453Asol}$. In previous studies, nuclear magnetic resonance (NMR) was used to measure a weak interaction between FMN and $MtrC_{sol}$ (13). Here, this technique was used to determine the interaction between FMN and the MtrC variants $MtrC_{C453Asol}$ and a variant MtrC with Cys_{453}

substituted with serine ($MtrC_{C453Ssol}$). The paramagnetic regions of the NMR spectra of $MtrC_{sol}$, $MtrC_{C453Ssol}$, and $MtrC_{C453Asol}$ show similar signal positions and line widths (Fig. S5A), indicating that the structure and dynamics of these proteins are similar. The ^{31}P NMR signal of FMN upon exposure to oxidized $MtrC_{C453Ssol}$ was monitored, and the data revealed that binding occurs in the slow exchange regime in the NMR timescale, indicating strong binding (Fig. S5B). These results show that substitution of the cysteine increases the affinity of oxidized MtrC for FMN.

$MtrC_{sol}$ can form an isolatable complex with FMN under anaerobic conditions in the presence of a thiol-reducing agent (17). The ability of $MtrC_{C453Asol}$ to form a similar complex was investigated by incubating $MtrC_{sol}$ or $MtrC_{C453Asol}$ with an excess of FMN and 1 mM dithiothreitol (DTT) under anaerobic conditions for 30 min before passage through a desalting column and fluorometric analysis (Fig. 3B). The fluorescent spectra of both MtrC were similar, showing that $MtrC_{C453Asol}$ would form a similar FMN complex to $MtrC_{sol}$ in the presence of DTT. DTT is typically used as a disulfide-reducing agent, and so, it was assumed that the role of DTT was to reduce the Cys_{444}-Cys_{453} disulfide, and this formed the MtrC-FMN complex. Substitution of Cys_{453} with alanine would prevent the disulfide from forming and remove the requirement of DTT for complex formation. However, when $MtrC_{C453Asol}$ was incubated with FMN in the absence of DTT, the purified fluorescent spectra of $MtrC_{C453Asol}$ were identical to $MtrC_{sol}$, showing that FMN had not bound (Fig. 3B). DTT is capable of reducing both FMN and heme, and it was possible that the interaction between MtrC and FMN also required the specific reduction of either MtrC and FMN. This was explored by incubating $MtrC_{C453Asol}$ or $MtrC_{sol}$ with FMN and 50 μM sodium dithionite. The fluorescence spectrum of the isolated complexes revealed copurification of FMN with $MtrC_{C453Asol}$ but not $MtrC_{sol}$ (Fig. 3C), consistent with the reduced forms of FMN and MtrC heme facilitating an increase in the affinity of FMN for $MtrC_{C453Asol}$. These data suggest that the interaction between FMN and MtrC is determined by the redox state of MtrC/FMN as well as the CX_8C motif.

Structural comparison of $MtrC_{sol}$ and $MtrC_{C453Asol}$. Biochemical analyses revealed that the CX_8C motif has an important role in controlling interactions between FMN and MtrC. When the disulfide bond is broken, either through reduction or mutagenesis, MtrC is more able to bind FMN, suggesting a conformational change that would affect the affinity of MtrC for FMN.

$MtrC_{C453Asol}$ was crystallized, and a structural model was determined to a resolution of 1.9 Å (Table S3). The overall structure was almost identical to the wild-type structure with a root mean square displacement (RMSD) of 0.297 Å (Fig. 4A and B). The area around Cys_{453} was largely conserved, although F_o-F_c maps revealed a negative patch of density where the disulfide was formed between Cys_{453} and Cys_{444} in $MtrC_{sol}$ (Fig. 4C). This confirmed that Cys_{453} was replaced with alanine and the disulfide was missing, but there were no other significant changes in the environment near residue 453. In addition, there was no electron density consistent with the covalent attachment of anything to Cys_{444} (Fig. 4C and D). These data show that the Cys_{453} substitution caused little perturbation of MtrC beyond the removal of the disulfide within the second β-barrel domain of MtrC. This surprising result did not explain how the removal of a disulfide bond could control binding and reduction of FMN.

One possible explanation for the discrepancy between the catalytic and structural differences could be that the crystal structure represents a stable conformation of the two MtrC isoforms and that a change in the conformational flexibility of MtrC causes the change in FMN interaction upon disulfide reduction. To investigate this further, samples of $MtrC_{sol}$ and $MtrC_{C453Asol}$ were analyzed using size exclusion chromatography combined with small-angle X-ray scattering (SEC-SAXS). Both samples eluted at the same positions and gave a uniform radius of gyration (R_g) across the peak (Fig. S6). Scaling and signal averaging of both samples gave scattering curves showing a high degree of similarity at low scattering factors (q), but as q increased, the two scattering curves deviated, suggesting a subtle difference between the two conformations (Fig. 5A).

Plotting the data as a function of $I \times q^2$ versus q (Kratky plot [Fig. 5B]) revealed profiles for both complexes consistent with folded proteins. Both samples were homogenous at

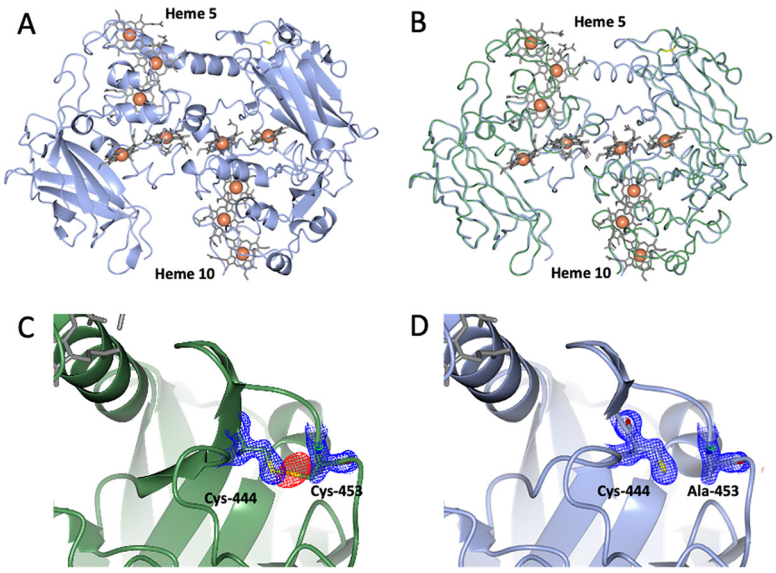

FIG 4 Crystal structure of $MtrC_{C453sol}$ (PDB accession no. 7QTH). (A) Cartoon representation of $MtrC_{C453sol}$. Hemes are shown as gray cylinders with the iron atoms represented as orange spheres. Cys-444 and Ala-453 side chains are shown as cylinders. (B) Structural superposition of the structure of $MtrC_{C453sol}$ (blue) with that of $MtrC_{sol}$ (green; PDB accession no. 4LM8). (C and D). $2F_o$-F_c (blue) and F_o-F_c (green/red) electron density maps, contoured at 1.2 and 3 sigma, respectively, resulting from refinement of coordinates for $MtrC_{sol}$ (C) and $MtrC_{C453sol}$ (D) against the $MtrC_{C453sol}$ data. For clarity, solvent molecules are not shown, and maps are clipped to within 2 Å of residues 444 and 453.

low *q*, but the slight increase in scattering at higher *q* suggested that $MtrC_{sol}$ was more flexible than $MtrC_{C453Asol}$. Distance distribution [*P*(*r*)] curves provided R_g and maximum dimension (D_{max}) values of 29.41 ± 0.14 and 91.2 Å for Mtr_{sol} and similar R_g and D_{max} values of 29.44 ± 0.14 and 91.5 for $MtrC_{C453A\text{-}sol}$ (Fig. 5C), indicating that both structures were very similar. The *P*(*r*) curves were finally used to generate structural models for both complexes using DAMMIN (20). These molecular envelopes fitted well to the data, with chi-square values of 1.133 and 1.124 for $MtrC_{sol}$ and $MtrC_{C453Asol}$, respectively (Fig. 5D). The molecular envelopes were then fitted to the MtrC crystal structure (Fig. 5E and F). Surprisingly, neither envelope matched the crystal structure. Normalized spatial discrepancy (NSD) values between the MtrC model and the molecular envelopes were 1.17 ($MtrC_{C453Asol}$) and 1.28 ($MtrC_{sol}$), suggesting that, while neither solution model fitted the structure perfectly, $MtrC_{C453Asol}$ in solution more closely resembles the crystal structure than $MtrC_{sol}$. These differences suggest solution-based transient conformations that may explain why $MtrC_{C453Asol}$ and $MtrC_{sol}$ show different affinities for FMN.

DISCUSSION

S. oneidensis MR-1 is known to encode over 40 different cytochromes and has a high concentration of intracellular iron (1, 21). In comparison to other bacteria, *S. oneidensis* is susceptible to damage from ionizing radiation. This susceptibility is not a consequence of direct radiation damage but indirect through the activation of several reactive species, notably ROS. It is most likely that the susceptibility of *S. oneidensis* MR-1 to ROS occurs due to the single-electron reduction of peroxide to hydroxyl radicals through the Fenton reaction catalyzed by Fe^{2+} available inside the cell (21). Under saturating oxygen conditions, *mtr* expression is likely to be suppressed; however, as the cell population increases, the oxygen concentration decreases and the expression of the *mtr* operon begins. For *S. oneidensis* pC453A, this would cause the formation of peroxide. This could explain the initial exponential growth phase that stops at an OD between 0.1 and 0.3.

To understand how the CX_8C motif in MtrC can protect against oxidative damage, a range of plasmids containing mutated *mtrC* genes were constructed and inserted into an *mtrC* knockout strain of *S. oneidensis*. The growth of MtrC variants unable to form

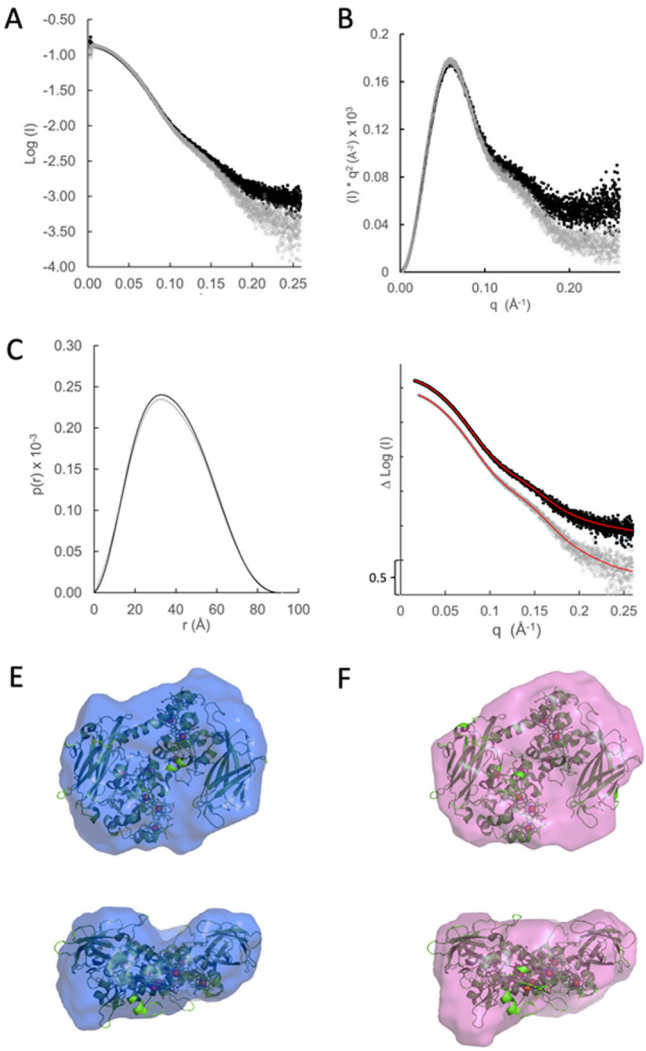

FIG 5 Small-angle X-ray scattering analysis of soluble MtrC (black) and $MtrC_{C453A}$ (gray). (A) Average scattering curves for $MtrC_{sol}$ and $MtrC_{C453Asol}$ showing a divergence at q values greater than 0.1. (B) Scattering data of $MtrC_{sol}$ and $MtrC_{C453Asol}$ plotted as $(I)\times q^2$ versus q (Kratky plot). (C) $P(r)$ distance distribution plot showing the probability distribution of both $MtrC_{sol}$ and $MtrC_{C453Asol.}$ (D) Molecular envelopes were generated from the scattering data using DAMMIN. The simulated curves for all data are shown in red. The DAMMIN curves fitted to the scattering data with chi-square values of 1.133 and 1.124 for $MtrC_{sol}$ and $MtrC_{C453Asol,}$ respectively. (E, F) The molecular envelopes of $MtrC_{C453Asol}$ (E) and $MtrC_{sol}$ (F) generated by DAMMIN were fitted to the MtrC crystal structure (PDB accession no. 4LM8). The NSD values between the MtrC crystal structure and $MtrC_{C453Asol}$ or $MtrC_{sol}$ were 1.28 and 1.17, respectively.

the Cys_{444}-Cys_{453} disulfide bond under aerobic conditions was severely impaired compared with the wild-type organism. The biphasic growth could be explained by the accumulation of hydrogen peroxide, reaching cytotoxic levels after 2 h and preventing further growth. After approximately 10 h, there was a second, recovery exponential phase once the bacteria no longer expressed recombinant MtrC. The best-expressed recombinant MtrC variant, $MtrC_{C453A}$, was as effective a goethite reductase as wild-type MtrC under the conditions tested, showing that the disulfide bond is not required for anaerobic mineral respiration.

In vitro analysis of soluble MtrC isoforms revealed that FMN reduction was responsible for the increased peroxide formed by $MtrC_{C453Asol}$ and the interaction between FMN and MtrC was controlled by both the redox state of the Cys_{444}-Cys_{453} pair and the redox state of FMN-MtrC. No changes were detected in the crystal structure of $MtrC_{C453Asol}$, suggesting that the effect of removing the disulfide caused changes to the stability of

MtrC, as indicated by SAXS experiments that showed differences in intensity at higher scattering angles. The structure of *Shewanella* MtrC is unusual in containing two multiheme domains (domains II and IV) separated by beta-barrel domain III containing the CX_8C motif. It would be possible to disrupt electron transfer between the two multiheme domains through movement of the region connecting domain II to domain III, close to the CX_8C motif. Molecular dynamic docking simulations indicated flavin was most likely to associate near heme 2 of domain II (15); however, it is not clear how this binding site would be affected by the redox state of the CX_8C motif some 30 Å away.

These results help to clarify the reason for the conserved disulfide bond on the surface of MtrC cytochromes. Under anaerobic mineral-respiring conditions, the MtrC disulfide can be reduced, increasing the association of secreted FMNs to the cytochrome and allowing effective reduction of FMN that can then reduce insoluble metal oxides. If the cell is exposed to oxygen, the two cysteines become oxidized and form a disulfide bond, which causes discrete conformational changes in MtrC and limits the association and reduction of FMN, which, in turn, prevents the FMN-mediated production of ROS. In our $MtrC_{C453A}$ isoform, the formation of the disulfide bond is prevented, trapping $MtrC_{C453A}$ into a state that favors FMN reduction under aerobic conditions, leading to increased production of peroxide and cell damage. The disulfide of MtrC therefore functions as a switch, changing the reactivity of MtrC on exposure to oxygen.

Shewanella species live in the waters and sediments of lakes, rivers, and oceans and consequently may experience rapid changes in the oxygen concentration of the immediate environment. Anaerobic expression of *mtrCAB* by *S. oneidensis* MR-1 allows the continuous flux of electrons generated inside the cell to access the surface of the cell, where they can be transferred to extracellular electron acceptors. Under aerobic conditions, these electrons would reduce oxygen, generating the ROS that then attack the cell. To minimize the risk of cellular damage, *S. oneidensis* exposed to oxygen must immediately decrease the rate of ROS production to concentrations that can be dealt with by the diheme peroxidases present in the periplasm. This surface-exposed CX_8C motif provides a rapid switching mechanism to prevent FMN reduction and allows *Shewanella*-containing MtrCAB to prevent the formation of ROS under aerobic conditions.

MATERIALS AND METHODS

Construction of strains. PCR was performed using primers listed in Table S1 in the supplemental material. For generation of cysteine mutants in the membrane-bound form of MtrC, plasmid pMtrC, a pBAD202/D-TOPO cloning vector containing the *mtrC* gene from *S. oneidensis* MR-1, was used (22). For generation of cysteine mutants in the soluble form of MtrC, a modified *mtrC* plasmid was used in which the nucleotide sequence encoding the lipid anchor site and signal peptide of MtrC was replaced with the signal peptide sequence of MtrB (pMtrCsol). A nucleotide sequence encoding a StrepTactin tag was inserted at the 3′ end of *mtrC* to give a C-terminal affinity tag.

Single-cysteine mutant plasmids served as the templates in further PCRs to generate double mutant *mtrC* where both cysteine residues were substituted for alanine. Plasmids are summarized in Table S2.

Either pMtrC, pC444A, pC453A, or pC444A, C453A was transformed into *S. oneidensis* Δ*mtrC* (LS661). The final strains generated are described and summarized in Table 1. *S. oneidensis* Δ*mtrC* (LS661) cell lines containing plasmids will be referred to as *S. oneidensis* pMtrC (native MtrC expressing), *S. oneidensis* pC444A (single-cysteine substitution at amino acid position 444), *S. oneidensis* pC453A (single-cysteine substitution at amino acid position 453), or *S. oneidensis* pC444A, C453A (double-cysteine substitution).

Growth of *S. oneidensis* strains. For aerobic growth curves, *S. oneidensis* strains were inoculated into LB cultures with 50 μg/mL kanamycin and 0 to 10 mM arabinose in a 96-well plate. This was incubated aerobically at 30°C in a FLUOstar Omega plate reader (BMG Labtech) under agitation. The OD_{600} was recorded at 30-minute intervals.

For anaerobic growth curves, LB medium was supplemented with 50 mM sodium fumarate to act as an electron acceptor in place of O_2. One-milliliter aliquots of cultures were transferred into a 48-well plate and transferred into an anaerobic glove box and left for 30 min. A coverslip was adhered before the plate lid was glued into place using an airtight adhesive. The plate was then removed from the glove box and incubated as described above but without agitation. A control well containing LB lacking sodium fumarate and inoculated with *S. oneidensis* MR-1 was used to confirm anaerobic conditions.

Indigo carmine assay for H_2O_2 measurements. *S. oneidensis* pMtrC and *S. oneidensis* pC453A were grown anaerobically in LB media with 50 mM sodium fumarate and 5 mM arabinose. Samples were removed before the cultures were supplemented with fresh LB media and grown aerobically for 2 h, and further samples were taken. Samples were taken and assayed for H_2O_2 using Oxygen Vacu-Vials kit K-7503 (CHEMetrics) after sparging with argon. Final samples were assayed after incubation with 0.3 U catalase and further sparging with

argon to remove oxygen formed from the process. The resulting reactions were analyzed at 610 nm with the absorbance of sparged samples before and after catalase incubation attributed to hydrogen peroxide.

Protein expression and purification. LB medium supplemented with 50 μg/mL of kanamycin and 20 mM sodium fumarate was sparged with nitrogen and inoculated with *S. oneidensis* strains. Cultures were incubated at 30°C with shaking, and cell growth was monitored. When OD_{600} had reached ~0.4, 5 mM arabinose was added to cultures, and oxygen was introduced to cultures before again being incubated at 30°C shaking at 220 rpm for a further 2 h. Afterward, cells were centrifuged and resuspended in 20 mM HEPES, pH 7.8, to an OD_{600} value of 0.5. Samples were analyzed using SDS-PAGE by the heme stain method to assess cytochrome expression levels.

Protein purification. *S. oneidensis* strains containing either pC453Asol, pMtrCsol, or pC453S were inoculated into LB media supplemented with 50 μg/mL kanamycin and 0.3 U/mL catalase and incubated at 30°C. When OD_{600} reached ~0.5, cultures were induced with 5 mM arabinose and incubated aerobically at 30°C for 10 h before centrifugal harvesting. Soluble MtrC isoforms were isolated as described previously (17). The detergent-solubilized $MtrC_{C453A}AB$ complex was isolated using a different method as described previously (23). Fractions were analyzed via SDS-PAGE using Coomassie and heme staining.

Crystallographic analysis of $MtrC_{C453Asol}$. $Mtr_{C453Asol}$ samples were concentrated to 10 mg/mL before crystallization using sitting-drop vapor diffusion with 30% polyethylene glycol 6000 (PEG 6000), 0.2 M sodium acetate pH 5, and 0.1 M calcium chloride. Crystals were harvested into cryo-protectant of 30% PEG 6000, 0.2 M sodium acetate, pH 5, 0.1 M calcium chloride, and 12% glycerol before vitrification in liquid nitrogen. X-ray diffraction data were collected at beamline I04 at Diamond Light Source (DLS). Crystals were of space group $P2_12_12_1$ with cell dimensions of a = 53.06 Å, b = 90.33 Å, and c = 154.81 Å and diffracted to a resolution of 1.86 Å. Data were collected over 180° with a 0.2° Ω oscillation per image and 0.1-s exposure per image with an unattenuated 32- by 20-μm beam. Data were integrated using XDS and scaled using Aimless from the CCP4 suite (24–26). The structure of $MtrC_{C453A\text{-}sol}$ was solved via molecular replacement using Phaser and MtrC (PDB accession no. 4LM8) as a search model. Alternating rounds of model building with COOT (27) and refinement using REFMAC5 were used to give a final model with an R_{cryst} (R_{free}) of 15.1 (19.6%) (28) (Table S3).

SEC-SAXS. $MtrC_{sol}$ and $MtrC_{C453Asol}$ were concentrated to 7.5 mg/mL in 20 mM HEPES, pH 7.5, and 50 mM NaCl and analyzed on beamline B21 at DLS. Samples were passed through a Shodex KW402.5-4F column at 0.16 mL/min, and data were collected in the form of scans from the eluent. Scattered X-rays were measured using an Eiger 4M detector. Data were analyzed using ScÅtter IV (https://bl1231.als.lbl.gov/scatter/). Six to 10 scans with uniform radius of gyration (R_g) values were averaged, and baseline was subtracted using baseline scans taken before the protein peak (Fig. S6).

Intensity of scattering factor Q curves (I(Q) curves) were analyzed using ATSAS software suite (29) to estimate the R_g and Kratky plots to evaluate the overall compactness of the protein complexes. GNOM (30) was used to calculate the pair-distance distribution function [$P(r)$] to provide an independent estimation of R_g and maximum dimension (D_{max}). *Ab initio* bead modeling using DAMMIN generated molecular envelopes of $MtrC_{sol}$ and $MtrC_{C453Asol}$, aligned to the *S. oneidensis* MtrC crystal structure using SUPCOMB (31).

Data availability. The C453A MtrC structure and the associated structure factors are deposited in the Protein Data Bank under accession no. 7QTH. Data sets used to make figures are deposited at figshare (https://figshare.com/articles/dataset/Baseline_subtracted_scattering_curves_of_soluble_MtrC_and_MtrC_C453A_in_20_mM_HEPES_50_mM_NaCl_pH_7_5/21781943).

SUPPLEMENTAL MATERIAL

Supplemental material is available online only.

FIG S1, JPG file, 0.02 MB.
FIG S2, JPG file, 0.02 MB.
FIG S3, JPG file, 0.02 MB.
FIG S4, JPG file, 0.02 MB.
FIG S5, JPG file, 0.02 MB.
FIG S6, JPG file, 0.02 MB.
TABLE S1, DOCX file, 0.01 MB.
TABLE S2, DOCX file, 0.01 MB.
TABLE S3, DOCX file, 0.01 MB.

ACKNOWLEDGMENTS

We thank Diamond Light Source for beamtime (proposal mx13467) and Nikul Khunti and other staff of beamlines I04 and B21 for assistance with data collection.

This research was supported by BBSRC grants BB/K009885/1 and BB/L023733/1 and an NRP BBSRC DTP studentship to M. P. Norman.

REFERENCES

1. Heidelberg JF, Paulsen IT, Nelson KE, Gaidos EJ, Nelson WC, Read TD, Eisen JA, Seshadri R, Ward N, Methe B, Clayton RA, Meyer T, Tsapin A, Scott J, Beanan M, Brinkac L, Daugherty S, DeBoy RT, Dodson RJ, Durkin AS, Haft DH, Kolonay JF, Madupu R, Peterson JD, Umayam LA, White O,

Wolf AM, Vamathevan J, Weidman J, Impraim M, Lee K, Berry K, Lee C, Mueller J, Khouri H, Gill J, Utterback TR, McDonald LA, Feldblyum TV, Smith HO, Venter JC, Nealson KH, Fraser CM. 2002. Genome sequence of the dissimilatory metal ion–reducing bacterium Shewanella oneidensis. Nat Biotechnol 20:1118–1123. https://doi.org/10.1038/nbt749.
2. Shi L, Squier TC, Zachara JM, Fredrickson JK. 2007. Respiration of metal (hydr)oxides by Shewanella and Geobacter: a key role for multihaem c-type cytochromes. Mol Microbiol 65:12–20. https://doi.org/10.1111/j.1365-2958.2007.05783.x.
3. Myers CR, Myers JM. 1997. Cloning and sequence of cymA, a gene encoding a tetraheme cytochrome c required for reduction of iron(III), fumarate, and nitrate by Shewanella putrefaciens MR-1. J Bacteriol 179:1143–1152. https://doi.org/10.1128/jb.179.4.1143-1152.1997.
4. Beliaev AS, Klingeman DM, Klappenbach JA, Wu L, Romine MF, Tiedje JM, Nealson KH, Fredrickson JK, Zhou J. 2005. Global transcriptome analysis of Shewanella oneidensis MR-1 exposed to different terminal electron acceptors. J Bacteriol 187:7138–7145. https://doi.org/10.1128/JB.187.20.7138-7145.2005.
5. Ross DE, Ruebush SS, Brantley SL, Hartshorne RS, Clarke TA, Richardson DJ, Tien M. 2007. Characterization of protein-protein interactions involved in iron reduction by Shewanella oneidensis MR-1. Appl Environ Microbiol 73:5797–5808. https://doi.org/10.1128/AEM.00146-07.
6. Richardson DJ, Butt JN, Fredrickson JK, Zachara JM, Shi L, Edwards MJ, White G, Baiden N, Gates AJ, Marritt SJ, Clarke TA. 2012. The 'porin-cytochrome' model for microbe-to-mineral electron transfer. Mol Microbiol 85:201–212. https://doi.org/10.1111/j.1365-2958.2012.08088.x.
7. Edwards MJ, White GF, Lockwood CW, Lawes MC, Martel A, Harris G, Scott DJ, Richardson DJ, Butt JN, Clarke TA. 2018. Structural modeling of an outer membrane electron conduit from a metal-reducing bacterium suggests electron transfer via periplasmic redox partners. J Biol Chem 293:8103–8112. https://doi.org/10.1074/jbc.RA118.001850.
8. Edwards MJ, White GF, Butt JN, Richardson DJ, Clarke TA. 2020. The crystal structure of a biological insulated transmembrane molecular wire. Cell 181:665–673.e10. https://doi.org/10.1016/j.cell.2020.03.032.
9. von Canstein H, Ogawa J, Shimizu S, Lloyd JR. 2008. Secretion of flavins by Shewanella species and their role in extracellular electron transfer. Appl Environ Microbiol 74:615–623. https://doi.org/10.1128/AEM.01387-07.
10. Marsili E, Baron DB, Shikhare ID, Coursolle D, Gralnick JA, Bond DR. 2008. Shewanella secretes flavins that mediate extracellular electron transfer. Proc Natl Acad Sci U S A 105:3968–3973. https://doi.org/10.1073/pnas.0710525105.
11. Shi Z, Zachara JM, Shi L, Wang ZM, Moore DA, Kennedy DW, Fredrickson JK. 2012. Redox reactions of reduced flavin mononucleotide (FMN), riboflavin (RBF), and anthraquinone-2,6-disulfonate (AQDS) with ferrihydrite and lepidocrocite. Environ Sci Technol 46:11644–11652. https://doi.org/10.1021/es301544b.
12. Wang ZM, Shi Z, Shi L, White GF, Richardson DJ, Clarke TA, Fredrickson JK, Zachara JM. 2015. Effects of soluble flavin on heterogeneous electron transfer between surface-exposed bacterial cytochromes and iron oxides. Geochim Et Cosmochim Acta 163:299–310. https://doi.org/10.1016/j.gca.2015.03.039.
13. Paquete CM, Fonseca BM, Cruz DR, Pereira TM, Pacheco I, Soares CM, Louro RO. 2014. Exploring the molecular mechanisms of electron shuttling across the microbe/metal space. Front Microbiol 5:318. https://doi.org/10.3389/fmicb.2014.00318.
14. Babanova S, Matanovic I, Cornejo J, Bretschger O, Nealson K, Atanassov P. 2017. Outer membrane cytochromes/flavin interactions in Shewanella spp.–a molecular perspective. Biointerphases 12:021004. https://doi.org/10.1116/1.4984007.
15. Breuer M, Rosso KM, Blumberger J. 2015. Flavin binding to the deca-heme cytochrome MtrC: insights from computational molecular simulation. Biophys J 109:2614–2624. https://doi.org/10.1016/j.bpj.2015.10.038.
16. Hong GY, Pachter R. 2016. Bound flavin–cytochrome model of extracellular electron transfer in Shewanella oneidensis: analysis by free energy molecular dynamics simulations. J Phys Chem B 120:5617–5624. https://doi.org/10.1021/acs.jpcb.6b03851.
17. Edwards MJ, White GF, Norman M, Tome-Fernandez A, Ainsworth E, Shi L, Fredrickson JK, Zachara JM, Butt JN, Richardson DJ, Clarke TA. 2015. Redox linked flavin sites in extracellular decaheme proteins involved in microbe-mineral electron transfer. Sci Rep 5:11677. https://doi.org/10.1038/srep11677.
18. Bechtel TJ, Weerapana E. 2017. From structure to redox: the diverse functional roles of disulfides and implications in disease. Proteomics 17:1600391. https://doi.org/10.1002/pmic.201600391.
19. Groitl B, Jakob U. 2014. Thiol-based redox switches. Biochim Biophys Acta 1844:1335–1343. https://doi.org/10.1016/j.bbapap.2014.03.007.
20. Franke D, Svergun DI. 2009. DAMMIF, a program for rapid ab-initio shape determination in small-angle scattering. J Appl Crystallogr 42:342–346. https://doi.org/10.1107/S0021889809000338.
21. Daly MJ, Gaidamakova EK, Matrosova VY, Vasilenko A, Zhai M, Venkateswaran A, Hess M, Omelchenko MV, Kostandarithes HM, Makarova KS, Wackett LP, Fredrickson JK, Ghosal D. 2004. Accumulation of Mn(II) in Deinococcus radiodurans facilitates gamma-radiation resistance. Science 306:1025–1028. https://doi.org/10.1126/science.1103185.
22. Shi L, Lin JT, Markillie LM, Squier TC, Hooker BS. 2005. Overexpression of multi-heme C-type cytochromes. Biotechniques 38:297–299. https://doi.org/10.2144/05382PT01.
23. Hartshorne RS, Reardon CL, Ross D, Nuester J, Clarke TA, Gates AJ, Mills PC, Fredrickson JK, Zachara JM, Shi L, Beliaev AS, Marshall MJ, Tien M, Brantley S, Butt JN, Richardson DJ. 2009. Characterization of an electron conduit between bacteria and the extracellular environment. Proc Natl Acad Sci U S A 106:22169–22174. https://doi.org/10.1073/pnas.0900086106.
24. Winn MD, Ballard CC, Cowtan KD, Dodson EJ, Emsley P, Evans PR, Keegan RM, Krissinel EB, Leslie AGW, McCoy A, McNicholas SJ, Murshudov GN, Pannu NS, Potterton EA, Powell HR, Read RJ, Vagin A, Wilson KS. 2011. Overview of the CCP4 suite and current developments. Acta Crystallogr D Biol Crystallogr 67:235–242. https://doi.org/10.1107/S0907444910045749.
25. Kabsch W. 2010. XDS. Acta Crystallogr D Biol Crystallogr 66:125–132. https://doi.org/10.1107/S0907444909047337.
26. Potterton L, Agirre J, Ballard C, Cowtan K, Dodson E, Evans PR, Jenkins HT, Keegan R, Krissinel E, Stevenson K, Lebedev A, McNicholas SJ, Nicholls RA, Noble M, Pannu NS, Roth C, Sheldrick G, Skubak P, Turkenburg J, Uski V, von Delft F, Waterman D, Wilson K, Winn M, Wojdyr M. 2018. CCP4i2: the new graphical user interface to the CCP4 program suite. Acta Crystallogr D Struct Biol 74:68–84. https://doi.org/10.1107/S2059798317016035.
27. Emsley P, Lohkamp B, Scott WG, Cowtan K. 2010. Features and development of Coot. Acta Crystallogr D Biol Crystallogr 66:486–501. https://doi.org/10.1107/S0907444910007493.
28. Murshudov GN, Skubak P, Lebedev AA, Pannu NS, Steiner RA, Nicholls RA, Winn MD, Long F, Vagin AA. 2011. REFMAC5 for the refinement of macromolecular crystal structures. Acta Crystallogr D Biol Crystallogr 67:355–367. https://doi.org/10.1107/S0907444911001314.
29. Franke D, Petoukhov MV, Konarev PV, Panjkovich A, Tuukkanen A, Mertens HDT, Kikhney AG, Hajizadeh NR, Franklin JM, Jeffries CM, Svergun DI. 2017. ATSAS 2.8: a comprehensive data analysis suite for small-angle scattering from macromolecular solutions. J Appl Crystallogr 50:1212–1225. https://doi.org/10.1107/S1600576717007786.
30. Semenyuk AV, Svergun DI. 1991. GNOM-a program package for small-angle scattering data-processing. J Appl Crystallogr 24:537–540. https://doi.org/10.1107/S002188989100081X.
31. Kozin MB, Svergun DI. 2001. Automated matching of high- and low-resolution structural models. J Appl Crystallogr 34:33–41. https://doi.org/10.1107/S0021889800014126.